Scientific Reports

https://doi.org/10.1038/s41598-026-62859-8

Article in Press

Acoustic wave speed in aerogels across material classes: density scaling from theory and experiments

Received: 21 May 2026

Accepted: 14 July 2026

Published online: 25 July 2026

Cite this article as: Rege A., Merillas B., Hopp-Zinke M. *et al.* Acoustic wave speed in aerogels across material classes: density scaling from theory and experiments. *Sci Rep* (2026). https://doi.org/10.1038/s41598-026-62859-8

Ameya Rege, Beatriz Merillas, Max Hopp-Zinke, Christian Scherdel, Petra Herman, Marina Schwan, Nina H. Borzecka, József Kalmár & Atul Bhaskar

Acoustic wave speed in aerogels across material classes: Density scaling from theory and experiments

Ameya Rege[1,3,*], Beatriz Merillas[2], Max Hopp-Zinke[3], Christian Scherdel[4], Petra Herman[5], Marina Schwan[3], Nina H. Borzecka[3], József Kalmár[5], and Atul Bhaskar[6]

[1]University of Twente, Department of Mechanics of Solids, Surfaces & Systems, P.O. Box 217, Enschede, 7500 AE, Netherlands
[2]University of Valladolid, Cellular Materials Laboratory (CellMat), Faculty of Science, Paseo de Belén 7, Valladolid, 47011, Spain
[3]German Aerospace Center (DLR), Institute of Frontier Materials in Earth and in Space, Linder Höhe, Cologne, 51147, Germany
[4]Center for Applied Energy Research, Magdalene-Schoch-Straße 3, Würzburg, 97074, Germany
[5]University of Debrecen, HUN-REN-DE Mechanisms of Complex Homogeneous and Heterogeneous Chemical Reactions Research Group, Department of Inorganic and Analytical Chemistry, Egyetem tér 1, Debrecen, H-4032, Hungary
[6]University of Southampton, Faculty of Engineering and Physical Sciences, Southampton, SO17 1BJ, United Kingdom
[*]ameya.rege@utwente.nl

ABSTRACT

Understanding the propagation of elastic waves in ultra-light porous solids is essential for linking their microstructure to macroscopic properties and mechanical performance. In this work, we present first an experimental study of longitudinal sound velocity in aerogels spanning a wide range of chemical structures and mesoscopic architectures, including polyurethane, polylactic acid, polyimide, flexible organo-silica, classical silica, and phenolic (resorcinol-formaldehyde) aerogels. Compression wave velocities were measured and correlated with bulk density to establish scaling relations across aerogel material families. While classical elasticity implies direct coupling between sound velocity in isotropic solids and elastic moduli, we then examine the extent to which such continuum relations remain valid in aerogels, whose structure is governed by hierarchical porosity, nanoscale connectivity, and bending-dominated network mechanics. Finally, we suggest measuring the Young modulus of aerogels from the acoustic wave speed as a non-destructive testing alternative.

Introduction

Aerogels are ultra-lightweight, highly nanostructured porous solids derived from gels in which the liquid phase is replaced by gas while preserving the solid network. Typical porosities exceed 90%, with pore sizes ranging from a few nanometers to micrometers. This unique nano- to meso-scale porous architecture is the key reason why aerogels exhibit exceptional thermal, mechanical, and acoustic properties. The thermal insulation characteristics of aerogels have been the focus of the majority of the classical literature on aerogels. This is owing to the extremely low thermal conductivity arising from the dampening of the gaseous thermal transport which is a consequence of the Knudsen effect.[1] However, in the past decade, investigations on the mechanical and acoustic properties of aerogels have been gaining significant attention.[2–5]

Aerogels are particularly attractive for sound insulation and acoustic damping, especially at low to mid frequencies where conventional porous materials often underperform. Aerogels have exhibited high sound absorption coefficient and low sound transmission. Sound propagation in aerogels is fundamentally different from dense solids or open foams due to strong solid-fluid coupling.[2] The dominant mechanisms in sound propagation in aerogels are linked with viscous dissipation, thermal losses, solid-gas coupling, scattering and multiple reflections. At sufficiently small pore sizes, Knudsen effects can emerge, modifying classical acoustic damping models and making aerogels particularly effective at higher frequencies.[6,7] Controlled synthesis of aerogels with a monomodal narrow pore size in the mesoporous range may shed more light on these possibilities, but most aerogels often exhibit macropores.

Consistent with open-porous materials, aerogels exhibit scaling laws for their mechanical properties such as the elastic

modulus. Gibson and Ashby[8] demonstrated a quadratic dependence of the density on the elastic modulus for open cell foams. Most aerogels show deviations from this quadratic behaviour, possibly because of differences in the architecture and deformation mechanisms in aerogels. While Gibson and Ashby linked the quadratic dependence to the bending dominated deformation of the cell wall struts, Aney et al.,[9] for aerogels, explained the deviations to be resulting from the topology of the network. Comparable to the mechanical properties, the thermal conductivity also exhibits scaling behaviour of both the solid and gaseous components with the density.[10,11] Weigold and Reichenauer[10] empirically proposed a factor of 2 between the scaling exponents of the elastic modulus and the solid component of the thermal conductivity for a model system of densified polyurea aerogel. Aney and Rege[11] confirmed this by proposing a network decomposition model where they additionally provided an explaination for the scaling behaviour of the gaseous component of the thermal conductivity.

The velocity of sound in a material is directly governed by its elastic stiffness and density for homogeneous isotropic solids. For a structured material with statistical isotropy, wave speed for wavelength much longer that the length scale of heterogeneity is likewise dependent on the *apparent elastic moduli* and the *apparent density*. In 3D isotropic elastic solids, propagation of elastic wave (i.e., sound in solid) is characterised by two fundamental velocities – velocity of longitudinal p-waves and transverse s-waves respectively, associated with compressive and shear waves in an infinite medium. Here we have used the term velocity of sound synonymously with the so-called *bar velocity*. Bar wave velocity is associated with longitudinal compression waves in a rod with free external surfaces and scales as $(E/\rho)^{1/2}$, where E is the Young's modulus and ρ the density. For all wave types, stiffer materials transmit mechanical disturbances faster, while higher-density materials slow them down. The relationship between s-wave speed (c_T), p-wave speed (c_L), and bar wave speed ($\bar{c}_L$) is that the bar wave speed is described in terms of functions that depend on the Poisson's ratio alone. Having made this distinction, we will restrict ourselves to the bar wave speed $\bar{c}_L$.

In this paper, we explore, both theoretically and by means of experimental measurements, the density-dependence of the sound velocity in aerogels. For this purpose, classical silica, flexible organo-silica marshmallow-like (here on termed marshmallow) (MA), polyimide (PIA), phenolic (resorcinol-formaldehyde) (RFA), polyurethane (PUA), polylactic acid (PLA) aerogels were synthesised and tested for their sound velocity. Given the recent interest in acoustic insulation characteristics of aerogels,[2] we build upon earlier foundational studies,[12] and revisit this topic as well as extend it.

Theory

Gibson and Ashby first addressed the structure-property relationship for porous materials when investigating the apparent mechanical properties of foams. Within their open-cell foam model, proposed in 1982, they make use of a unit cell, cubic in nature whose edges are made up of prismatic bars.[8] Subjecting the bars to bending and considering the Euler-Bernoulli beam theory for slender beams, the following relations are deduced. The relative density scales with the dimensions of the bars as

$$\frac{\bar{\rho}}{\rho_s} \propto \left(\frac{t}{l}\right)^2, \tag{1}$$

where $\bar{\rho}$ is the *apparent* density (also known as bulk density) and ρ_s is the skeletal density, namely the density of the constituent material making up the bars (cell/pore walls). Here, l is the characteristic length of these bars, and t their thickness. Applying the Euler-Bernoulli beam theory, one can show for 3D solid foams with bending-dominated architecture that

$$\frac{\overline{E}}{E_s} \propto \left(\frac{t}{l}\right)^4, \tag{2}$$

where $\overline{E}$ is the *apparent* Young's modulus of the porous material and E_s is the Young's modulus of the constituent solid material making up the slender bars within the solid network. One can, therefore, express the relation between $\overline{E}$ and $\bar{\rho}$ as

$$\frac{\overline{E}}{E_s} \propto \left(\frac{\bar{\rho}}{\rho_s}\right)^2. \tag{3}$$

This quadratic relation is found to be correct in many open-porous foam-like materials. However, it has been observed that the scaling is not always quadratic. Two primary reasons for this departure from the quadratic exponent are: (i) the network topology may be kinematically (fully or partially) rigid, leading to a stretch-dominated deformation mechanism, and (2) the bars may not be slender, so an inevitable shear deformation that is not associated with quadratic scaling may exist. If one only considers buckling of the bars (cell walls), one gets an exponent of 1. Therefore, it seems reasonable to get a near quadratic relation for rigid foam-like materials and between 1 and 2 for more elastic foams. However, some materials exhibit scaling

beyond an exponent of 2 or even 3 or in some cases nearing 4.[8,9,13,14] In these cases, the cell wall morphology or the mode of deformation of the wall does not play a significant role in this deviation from 2, rather the topology of the network is crucial. Therefore, in general, it is convenient to express the scaling law in a more generalised form

$$\frac{\overline{E}}{E_s} \propto \left(\frac{\bar{\rho}}{\rho_s}\right)^m, \tag{4}$$

where m is the scaling exponent for modulus-porosity scaling. The acoustic properties are closely related to the elastic properties. For continua, the longitudinal bar velocity (to be referred to as the sound velocity) is given by

$$(c_L)_s = \sqrt{\frac{E_s}{\rho_s}}. \tag{5}$$

One can similarly express the bar velocity for long waves in porous media, by replacing modulus and density by the apparent modulus and the apparent density, as

$$\bar{c}_L = \sqrt{\frac{\overline{E}}{\bar{\rho}}}. \tag{6}$$

If the quotient $(\overline{E}/E_s) \sim \phi^m$, where ϕ is the relative density, namely, $\phi = \bar{\rho}/\rho_s$ then the bar velocity for long waves in a porous material would scale as per

$$\bar{c}_L \approx \left(\frac{\phi^m}{\phi}\right)^{\frac{1}{2}} = \phi^{\frac{(m-1)}{2}}. \tag{7}$$

This equation is valid for waves with wavelengths $\lambda \gg l_c$, where l_c denotes the characteristic length of non-homogeneity. Else when the wavelength starts becoming comparable with the length scale of heterogeneity then Eq. 6 is no longer valid due to several reasons, e.g., scattering. Since the measurements were performed at $f = 0.5$ MHz, the corresponding wavelength λ can be estimated from

$$\lambda = \frac{\bar{c}_L}{f}. \tag{8}$$

Using the measured range of bar velocities, the wavelengths lie between 0.1-1.5 mm. This range is orders of magnitude higher than the mean pore size of SA, RFA, PUA, PLA, PIA (typically mesoporous materials, namely pore sizes between 2-50 nm), and 1-2 orders of magnitude higher than MA. This establishes the validity of the long wave assumptions inherent in our work. Therefore one can define the relation between the scaling exponent, say a in the power-law scaling for the compression wave speed and the scaling exponent m from the scaling of the elastic modulus as

$$\bar{c}_L \propto \phi^a : \text{where } a = \frac{m-1}{2}. \tag{9}$$

Results

Aerogels of different chemical composition, nanoporous structures, and porosities were synthesised and tested for the compression sound waves propagation through them as outlined in the Methods section. Results are displayed in Fig. 1. Sound velocity measurements on 22 samples of aerogels – each in triplicate (thus for 66 measurements), with uncertainties mapped by error bars in the plot – are organised in one place here, relating wave speed with porosity for each material. To establish this relationship experimentally, porosity was the only parameter varied, while all other material and processing parameters were kept strictly constant. This ensured that the measured relationship reflects the effect of porosity alone. Given that bulk density is more intuitive and directly measurable, we plot compression acoustic wave speed, in particular, the bar velocity ($\bar{c}_L$) vs. bulk (or apparent) density ($\bar{\rho}$). The exponent a remains unaffected whether $\bar{c}_L$ is plotted against $\bar{\rho}$ or the relative density ϕ (Eq. 8).

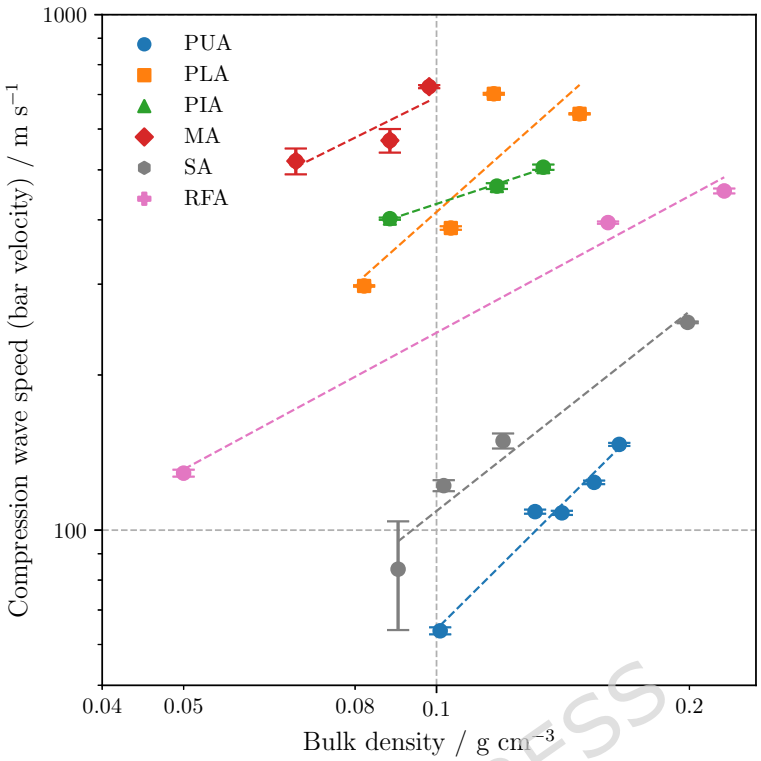

Figure 1. Compression sound wave speed (bar velocity) vs. bulk density plot of all measured aerogels. For every density, measurements were done in triplicate resulting in 66 measurement points. The uncertainties are reflected from the error bars. The trendlines demonstrate the power-law fit for each aerogel type. The exponents are tabularised in Table 1. PUA: polyurethane aerogels, PLA: polylactic acid aerogels, PIA: polyimide aerogels, MA: marshmallow aerogels, SA: silica aerogels, and RFA: resorcinol-formaldehyde aerogels.

Aerogel type	Measured a	Theoretical a	m from Eq. 4
PUA	$1.62_{\pm 0.01}$	$1.60_{\pm 0.25}$	$4.20^{\pm 0.5}$ (ref. own work and[15])
PLA	$1.44_{\pm 0.02}$	$1.46_{\pm 0.06}$	$3.92^{\pm 0.12}$ (ref. own work and[16])
PIA	$0.54_{\pm 0.06}$	$0.55_{\pm 0.08}$	$2.20^{\pm 0.15}$ (ref. own work and[17,18])
MA	$0.85_{\pm 0.09}$	$0.80_{\pm 0.10}$	$2.60^{\pm 0.20}$ (ref. own work and[19])
SA	$1.27_{\pm 0.05}$	$1.25_{\pm 0.10}$	$3.50^{\pm 0.20}$ (ref. own work and[20–22])
RFA	$0.86_{\pm 0.06}$	$0.85_{\pm 0.10}$	$2.70^{\pm 0.20}$ (ref. own work and[23])

Table 1. Comparison of the scaling exponent in the relation between the sound velocity and density as measured experimentally and as derived theoretically using Eq. 8. The exponent m from Eq. 4 is also tabularised to show the value being input in Eq. 8. PUA: polyurethane aerogels, PLA: polylactic acid aerogels, PIA: polyimide aerogels, MA: marshmallow aerogels, SA: silica aerogels, and RFA: resorcinol-formaldehyde aerogels.

An immediate observation is that SA and PUA demonstrate high compliance having very low sound velocities around or below 100 m s^{-1}. A power-law fit was generated for each of the aerogel dataset. The results are presented in Table 1.

The exponents for the experimentally measured values were obtained from the power-law fits for each directly measured sound velocity-porosity trend in Fig. 1. For the theoretical calculations, Eq. 8 was used in conjunction with *independently measured* apparent modulus and apparent density, ensuring that porosity is the only changed parameter for a given material. The exponent m for the elastic modulus vs. density for the different aerogels was used from our own data in validation with previously reported measurements as follows. PUA exhibited $m = 4.2$ which falls close around a 10% error to e.g., 3.7 as reported by Diascorn et al.[15] PLA showed $m = 3.92$ which is very close to the reported value of 4.04 by Lledó et al.[16] An exponent of $m = 2.2$ was obtained for PIA, which is also in agreement with the results from Meador et al.[18] and Filiminova

et al.[17] MA exhibited $m = 2.6$ which agrees with the results from Steffens et al.[19] For SA synthesised with this recipe, it is well known from a vast source of literature that the scaling exponent $m = 3.5 \pm 0.2$.[20,22,24] For RFA synthesised from this recipe, the exponent $m = 2.7 \pm 0.2$ was reported.[23] These above-mentioned values were used within Eq. 14 that provides an indirect but independent "theoretical" estimate for c_L. The theoretical scaling exponents for the compression sound waves thus calculated are displayed in Tab. 1. The directly measured experimental results for the sound velocity are in excellent agreement with the theoretical calculations.

Discussion

The results establish the validity of Eq. 7 for aerogels that are nanostructured materials. Important is also the validity of Eq. 6 that makes assumptions of an apparent medium replacing the aerogels that possesses complex skeletal architecture. Aerogels, in principle, violate almost every assumption behind classical elasticity. They exhibit extreme porosity, hierarchical non-homogeneity, and strong solid-fluid coupling. The aerogels studied in this paper exhibit totally different morphologies with respect to each other and span over different pore scales (refer to scanning electron microscopy images in Fig. S1 of the Supplementary Material). Despite these features, the use of such simple models remain valid for estimating the relation between acoustic and mechanical properties. However, to understand sound propagation in aerogels including the role of the microstructure, one might have to look into Biot's poroelastic model as well as frequency-dependent dispersive behaviour of aerogels and derive explicit expressions for the compression and shear wave speeds.[25–27]

From another perspective, one can exploit the validity of Eq. 6 for aerogels, to calculate the elastic modulus in those aerogels, given that majority of the aerogels, and all reported in this study, exhibit isotropic properties at the macroscopic scale. While a seemingly simple problem, it is challenging to obtain perfect cubes or cylinders for most types of aerogel monoliths, and even when produced, they are seldom crack or defect free. Due to these challenges, the stress-strain curve obtained for aerogels under uniaxial compression measurements is often not perfectly linear in the infinitesimal deformation regime. Moreover, initially warped coupons due to the practical difficulty in fabricating perfectly flat samples lead to measured stress-stress response that is much softer than the actual. Compressive tests are also frequently carried out on polymer aerogels, which suffer from the aspect ratio of the sample being limited by the possibility of buckling, thus resulting in a measurement that does not well represent unidirectional state of stress. These lead to estimating a value for the Young's modulus from the slope of the stress-strain curve in the infinitesimal strain region which does not correctly represent material stiffness. An interested reader is referred to the chapter on Mechanical Characterization of Aerogels in the Springer Handbook of Aerogels.[28] By contrast, no significant geometric constraints apply to testing the sound velocity. It can, therefore, be recommended to test sound velocity in aerogels, and use it to indirectly measure their elastic modulus using Eq. 6. Furthermore, the Young's modulus reported in this work is inferred from the measured longitudinal bar-wave velocity using one-dimensional elastic wave theory. For materials exhibiting viscoelastic behaviour, the modulus obtained by ultrasonic measurements may differ from the quasistatic modulus determined from conventional compression tests because of possible frequency dependence. Accordingly, the proposed method provides a rapid, non-destructive estimate of the effective elastic modulus under the measurement conditions and should not be interpreted as a universal replacement for quasistatic mechanical testing without appropriate validation.

For homogeneous isotropic materials, the p-wave velocity c_L depends on two independent elastic constants (any two of Young's modulus, Poisson's ratio, bulk modulus, or shear modulus, or Lame's constants, for example) the bulk modulus κ and shear modulus μ, and not only on E. Therefore, one needs to know the apparent Poisson ratio (or another additional apparent elastic constant) of the material, the aerogel in this case, in order to determine this second fundamental wave speed. Therefore, it is recommended, in addition to c_L, to either measure the Poisson ratio $\overline{\nu}$ also, or to measure the shear wave speed c_T. Future work will investigate the feasibility of measuring c_T, which, in principle, would enable direct determination of the effective shear modulus and complete elastic characterization. However, owing to the extremely low shear stiffness, high attenuation, fragile microstructure, and challenges associated with shear-wave coupling and signal identification in highly porous aerogels, such measurements are expected to be experimentally demanding. Accordingly, this remains an important direction for future research. Measuring c_T under the above-mentioned assumptions would yield the shear modulus

$$c_T = \sqrt{\frac{\overline{\mu}}{\overline{\rho}}}. \tag{10}$$

Therefore, if one measures c_T and $\overline{\nu}$, the apparent Young's modulus

$$\overline{E} = 2\overline{\mu}(1+\overline{\nu}) = 2\overline{\rho}c_T^2(1+\overline{\nu}). \tag{11}$$

On the other hand, if one measures c_T and c_L, the Young's modulus

$$\overline{E} = \frac{9\overline{\kappa}\overline{\mu}}{3\overline{\kappa}+\overline{\mu}}, \tag{12}$$

where $\overline{\kappa}$ can be expressed as

$$\overline{\kappa} = \bar{\rho}c_L^2 - \frac{4}{3}\bar{\rho}c_T^2. \tag{13}$$

Therefore, one can express $\overline{E}$ purely in terms of the compression and transverse sound velocities as

$$\overline{E} = \bar{\rho}\, c_T^2 \left(\frac{3c_L^2 - 4c_T^2}{c_L^2 - c_T^2}\right). \tag{14}$$

The above-proposed ideas rely on the applicability of continuum (classical) elasticity, which may not be considered *a priori* for aerogels because of their extreme porosity, hierarchical microstructure, and pronounced structural heterogeneity. The measurements, however, as shown in this study for a diverse range of aerogels, demonstrate alignment with classical elasticity.

Another brief point stemming from the discussion above and in relation to the significant literature by the then team of Fricke is as follows. Fricke et al.[12] used the following relation to compare stiffness and $\bar{c}_L$,

$$C_{11} = \bar{\rho}c_L^2. \tag{15}$$

While this is correct, one must note that C_{11} is not the Young's modulus $\overline{E}$. C_{11} is the longitudinal stiffness component of the fourth-order stiffness tensor $\mathbb{C}$. Since we experimentally measure $\overline{E}$ and not C_{11}, it is recommended to use the Eq. 13 to calculate the Young's modulus from c_L and c_T for comparative purposes against experimental data.

The measurement of moduli of elasticity, e.g. Young's modulus, Poisson's ratio, shear modulus, etc., using static testing is particularly demanding given the constraints encountered in sample preparation for soft materials such as aerogels. By contrast, these limitations are less severe for the measurement of sound velocity. Thus, our methodology here provides a convenient approach for the metrology of material properties for this class of materials, especially when the sample quantity and the possibility of shaping them into samples for static testing (such as coupons or in dog bone shapes) are limited. Alternatively, the wave speed-porosity scaling could be calibrated to measure the porosity of aerogels indirectly from density and sound velocity measurements, thus enhancing the value of our work.

Conclusions

In this short paper, we experimentally determined the longitudinal compression wave velocity in a series of aerogels bars, selected to span a broad spectrum of chemistries and structural architectures, including polyurethane, polylactic acid, polyimide, marshmallow, silica, and resorcinol-formaldehyde systems. The materials studied cover both organic and inorganic aerogel families, enabling a comparative assessment across distinct network morphologies. Among the tested systems, silica and polyurethane aerogels exhibited the strongest sound-insulating characteristics, with longitudinal wave speeds as low as 84 m s^{-1} and 64 m s^{-1}, respectively, for the lowest-density samples. These remarkably low wave velocities highlight the extreme mechanical compliance of ultra-light aerogel networks.

A central focus of this work was the investigation of density-dependent scaling laws governing acoustic wave propagation. Porous solids, including aerogels, are known to follow power-law scaling relations between elastic modulus and density, typically with exponents between 2 and 4, reflecting bending-dominated network mechanics. By combining classical elasticity relations for compression waves with experimentally determined density-modulus scaling, we established a direct relationship between the scaling exponent of the acoustic wave velocity and that of the elastic modulus. The theoretical predictions derived from continuum elasticity were found to agree remarkably well with experimental observations. This agreement demonstrates that the effective macroscopic elastic response of the investigated aerogels can be accurately described by homogenized continuum elasticity, despite their extreme porosity, hierarchical microstructure, and broad distribution of pore and ligament sizes.

Finally, we discussed the potential of sound velocity measurements as an indirect and non-destructive method for estimating elastic modulus in aerogels. This approach is particularly attractive given the experimental challenges associated with conventional mechanical testing of ultra-light porous materials, where sample preparation, microcracking, and structural defects often compromise reproducibility. Acoustic characterization thus offers a robust non-destructive alternative route for probing the effective stiffness of fragile aerogel networks.

Methods

Synthesis and structural characterisation of aerogels

Polyurethane aerogels

Polyurethane aerogel (PUA) samples were synthesized following the procedure reported by Merillas et al.[29,30] via polycondensation of pentaerythritol (purity >98 % - Alfa Aesar) and polymeric diphenylmethane diisocyanate (IsoPMDI 92140 - BASF Polyurethane) in solution with varying contents of potassium octoate (KOSMOS 75 MEG - Evonik) as a catalyst. Pentaerythritol was dissolved in dimethyl sulfoxide at a concentration of 100 g/L and was poured into a p-MDI solution of 44 g/L in 65:35 acetonitrile/tetrahydrofuran (molar ratio polyol/isocyanate of 0.43). The amount of a catalyst solution (70 g/L in THF) varied from 1 to 15 wt.% with respect to the total mass of precursors. The resulting mixture was stirred at 500 rpm for 20 s at room temperature and poured into a container. The resulting gels were subsequently covered with acetonitrile for 24 h and washed twice with the same solvent. Finally, gels were dried by supercritical CO_2 drying at 50 °C and 100 bar. The fabrication of PU aerogels followed a robust and standardized sol-gel procedure, consistently yielding materials with high structural integrity and reproducibility. The resulting particulate structures are intrinsically isotropic, exhibiting a narrow particle size distribution.[30,31]

Polylactic acid aerogels

Polylactic acid aerogels (PLA) were produced as described by Lledó et al.[16] via thermal-induced phase separation (TIPS). Different PLA contents with a molecular weight of 138 kg/mol (PLA LUMINY L130 provided by TotalEnergies Corbion (Gorinchem, The Netherlands) with L-isomer content >99 %) were dissolved in a solvent mixture (63:37 1,4-dioxane/EtOH) at 65 °C. The PLA content was compressed between 0.03 and 0.14 g/L. Then, the solution was poured into a container, which was placed in a freezer at −32 °C for 3 h. After solvent exchange by immersing the gels in cold ethanol at 8 °C for 24 h, samples were supercritically dried with CO_2 at 32.5 °C and 150 bar. PLA aerogels produced via a TIPS method driven by spinodal decomposition (liquid-liquid phase separation) exhibit highly homogeneous architectures, composed of nanofibrillar networks that show no directional dependency within the porous matrix.[32]

Polyimide aerogels

Polyimide aerogels (PIA) were synthesized by the sol-gel method following the procedure from Meador et al.[33] 4,4'-oxidianiline (4.05 g, 20.2 mmol) was dissolved in 78.6 mL (0.816 mol) of anhydrous N-methyl-2 pyrrolidinone (NMP) under continuous moderate stirring, which was maintained throughout the synthesis until casting. Biphenyl-3,3',4,4' - tetracarboxylic dianhydride (6.27 g, 21.3 mmol) was then introduced into the solution and stirred until a clear and homogeneous mixture was obtained. Separately, 1,3,5-triaminophenoxybenzene (0.183 g, 0.456 mmol) was dissolved in 25.1 mL (0.260 mol) of anhydrous NMP and subsequently added to the reaction mixture. Chemical imidization was initiated by the simultaneous addition of acetic anhydride (16.2 mL, 0.172 mol) and pyridine (13.8 mL, 0.172 mol). After 1-2 min, once complete dissolution was achieved, the resulting homogeneous sol was carefully poured into Teflon moulds, which were then sealed with Teflon lids. Gelation occurred within approximately 15–20 min. The formed gels were demoulded and aged in fresh NMP for 24 h. Solvent exchange was then carried out every 24 h using progressively higher acetone concentrations. Residual water was removed using a continuous solvent extraction and regeneration system. Acetone was initially extracted with liquid CO_2 at 50 bar and room temperature, followed by supercritical CO_2 drying at 90-100 bar and 60 °C. By adjusting the solid-to-solvent ratio in this synthesis protocol, three polyimide aerogels with distinct bulk densities were obtained, as summarized in Table 2. The synthesis protocol employed for the preparation of the PI aerogels is a well-established, validated, and highly reproducible method that has been used for decades in numerous studies.[17,34,35] The samples prepared in this work are highly reproducible regarding both structure and properties. PI aerogels are isotropic, as no directional dependence has been observed either in their microstructure, or mechanical, optical, thermal properties.[17,34,35]

Marshmallow aerogels

The marshmallow aerogels (MA) were prepared following the procedure of Fener and Niemeyer,[36] which is based on the original discovery by the team led by Hayase and Kanamori in 2011.[37] First, urea granulate (4.06 mol equivalent to methyltrimethoxysilane) was dissolved in a mixture of demineralised water (40.67 mol eq.) and glacial acetic acid (3.56×10^{-3} mol eq.) at 50 °C under continuous stirring. Once a homogeneous solution was obtained, a hexadecyltrimethylammonium chloride solution (25 wt. % in water, 0.12 mol eq.) and methyltrimethoxysilane (1.00 mol eq.) were added and stirring was continued for 15 min at 50 °C. Then, dimethoxydimethylsilane (0.69 mol eq.) was added and the mixture was stirred for an additional 45 min at 50 °C. The solution was poured into a 3D-printed cylindrical casting mould (90 mm inner diameter, TPU filament) where gelation occured during heat treatment at 80 °C for 24 h. After gelation, the cylindrical sample was carefully demoulded and subjected to a six-step washing procedure: twice with demineralised water, twice with ethanol and twice again with demineralised water. Each step lasted approximately 8 h, with continuous stirring of the solvent for faster exchange. Within each step, twice the sample volume of solvent was used. Finally, the sample was dried in an oven at 80 °C for 24 h and cut using razor blades

and a 3D-printed cutting template to yield cylindrical discs with a height of 12 mm. The recipe for synthesising MA is well established and reproducible, as shown in our previous works.[5,19] The aerogels produced are isotropic and show no directional dependency for their mechanical properties.[5]

Silica aerogels

Tetraethyl orthosilicate (TEOS) aerogels (SA) were synthesized by hydrolysing TEOS in an ethanol–water mixture. The molar ratios of precursor, water and solvent were varied within the following ranges 1.00 : 7.7-11.6 : 9.4-7.7. The upper and lower bounds correspond to the tuning of the aerogel network density. First, TEOS was dissolved in ethanol (EtOH) and stirred magnetically at 150 rpm at room temperature. Subsequently, the mixture was then heated to 50°C, at which point an aqueous solution of 0.01 M HCl was added to initiate hydrolysis. After the addition, the solution was stirred for another 40 min while maintaining 50 °C, followed by five minutes of cooling while continuously stirring. Due to addition of 0.1 M NH_3 the gelation was initiated. The resulting mixture was placed in an air-tight container, in an oven at 50 °C for 24 h to allow gelation and aging. After these steps, the wet gel was carefully transferred to an ethanol washing bath. The solvent exchange was carried out in three 24-hour cycles at room temperature. Finally, the samples were dried by supercritical CO_2 extraction. The method for SA preparation aligns with majority of the classical literature and the reproducibility is outlined in a multitude of studies.[38] These aerogels are well-known to be isotropic at the macroscopic level.[39–42]

Aerogel	Bulk density [g cm^{-3}]	Skeletal density [g cm^{-3}]
PUA	0.101	
	0.131	
	0.141	1.170
	0.154	
	0.163	
PLA	0.082	
	0.104	1.240
	0.117	
	0.148	
PIA	0.088	
	0.118	1.444
	0.134	
MA	0.068	
	0.088	1.239
	0.098	
SA	0.090	
	0.100	1.690
	0.120	
	0.200	
RFA	0.050	
	0.160	1.400
	0.220	

Table 2. Apparent (bulk) densities and skeletal densities of the measured aerogels. PUA: polyurethane aerogels, PLA: polylactic acid aerogels, PIA: polyimide aerogels, MA: marshmallow aerogels, SA: silica aerogels, and RFA: resorcinol-formaldehyde aerogels.

Phenolic (resorcinol-formaldehyde) aerogels

Resorcinol-formaldehyde (RF) gels were synthesized by reacting resorcinol R (98 %, Aldrich) with formaldehyde F (24 % w/w (Carl Roth) in deionized water W, using sodium carbonate C as a catalyst. The R/W molar ratios were tailored from 0.003-0.021, while the R/C and R/F molar ratios were kept constant at 200 and 0.5, respectively. Following initial homogenization at room temperature (150 rpm), the solutions were sealed in polypropylene containers and cured at 60 °C for 7 days (Memmert GmbH, Germany). The resulting wet gels were cooled and submerged in an acetone bath; the solvent was replaced six times over 3 days to ensure complete water removal. Supercritical drying was performed with CO_2 (purity $\geq$ 99.995%, Praxair) in an autoclave of 60 L volume (Eurotechnica, Germany) at 60 °C and 110 bars for about 21 h. The degassing rate was adjusted to 0.2 bars per minute. The recipe used to prepare RF aerogels is well established in the literature and is reproducible.[43,44] These

aerogels were proven to exhibit isotropic properties.[45]

Density measurement

The bulk densities were measured using a GeoPyc instrument based on displacement measurement techniques (Micromeritics, Germany). The skeletal density was measured using an AccuPyc gas pycnometer (Micromeritics, Germany) with helium as the displacement gas.

Sound velocity testing setup

The sound velocity measurements for the PIA, MA, SA, and RFA were performed using an ultrasonic transit time equipment, developed in-house at CAE in Würzburg, Germany, consisting of two piezoelectric crystals serving as a transmitter and a receiver, respectively.[46] A major challenge lies in achieving effective acoustic coupling between the ultrasonic transducers and the aerogel specimen, since conventional wetting agents can damage the delicate porous structure. Therefore, the measurements were performed without the use of any coupling medium. This approach required some special constructive efforts to ensure effective coupling of waves into the highly porous aerogel. The receiver is mounted on a sled (see Fig. 2), allowing controlled application of variable contact loads onto the specimen. This also is useful for adjusting according to the sample size. Since many aerogels are highly susceptible to compression and only small loads could be applied, particular attention was paid to minimising friction in the sled mechanism. The aerogel sample is clamped between the transmitter and the receiver during the measurement. The transmitter piezoelectric crystal is excited to longitudinal oscillations by a high-frequency pulse, while the second crystal (the receiver) detects the arrival of the pulse excitation, so that the sound velocity can be calculated from the quotient of travel time and distance. The travel time of the ultrasonic pulse is determined using an oscilloscope with a relative measurement accuracy of 5 %. The sample thickness is measured with a dial gauge mounted between the transmitter and receiver with an accuracy of 0.2 mm. The frequency of the longitudinal sound waves is 0.5 MHz.

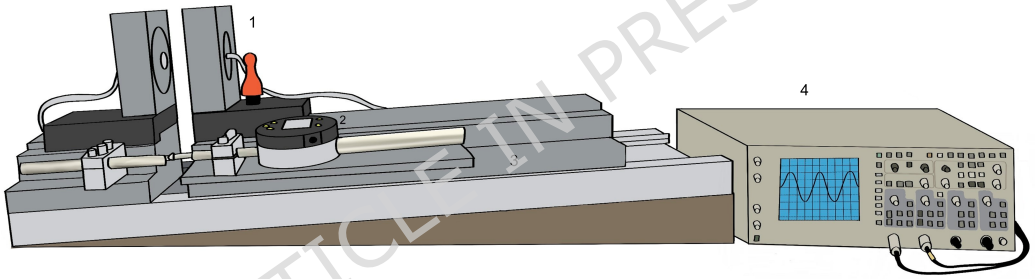

Figure 2. Ultrasound measurement set-up at CAE: the sample is clamped between transmitter and receiver (1) where the receiver is mounted on a rail (3). The sample thickness is measured with a dial gauge (2) and the runtime determined with an oscilloscope (4).

The sound velocity measurements for PUA and PLA were obtained by a pair of non-focused air-coupled ultrasonic transducers (developed at ITEFI-CSIC[47,48]) with the same frequency as that used for the other aerogel samples of 0.5 MHz, −20 dB relative bandwidth of 75 % and 20 mm aperture. These measurements were carried out at the ITEFI-CSIC, in Madrid, Spain. The transducers operate in a through-transmission configuration, positioned face-to-face, and the aerogel specimen is located between them at normal incidence. Signals with and without a sample between transducers were received and acquired, allowing the calculation of the ultrasound velocity in the sample from the velocity in the air, sample thickness, and the difference in time of flight between both cases. This difference can be calculated from the edge detection, the maximum in the cross-correlation between both signals, or the phase difference.

All the aerogel samples were prepared ensuring parallel surfaces for the sound velocity tests. All sound velocity measurements were made in triplicate. The reported error bars in Fig. 1 represent the standard deviations calculated from data obtained through independent measurements of 3 different aerogel specimens.

References

1. Koebel, M., Rigacci, A. & Achard, P. Aerogel-based thermal superinsulation: an overview. *J. sol-gel science technology* **63**, 315–339 (2012).
2. Budtova, T. *et al.* Acoustic properties of aerogels: current status and prospects. *Adv. Eng. Mater.* **25**, 2201137 (2023).

3. Gómez Álvarez-Arenas, T. *et al.* Viscoelasticity of silica aerogels at ultrasonic frequencies. *Appl. physics letters* **81**, 1198–1200 (2002).

4. Parale, V. G. *et al.* Mechanically strengthened aerogels through multiscale, multicompositional, and multidimensional approaches: a review. *Adv. Mater.* **36**, 2307772 (2024).

5. Zinke, M., Milow, B., Seide, G. & Rege, A. Mechanical structure-property relations in flexible silica-aerogels. *Mech. materials* **211**, 105510 (2025).

6. Hesse, C., Allebrodt, P. & Rege, A. Multi-Physikalische Untersuchungen zum Transmissionsverhalten neuartiger Kabinenseitenwände. *Deutscher Luft-und Raumfahrtkongress 2020* (2020).

7. Martín-de León, J. *et al.* Beyond geometrical scaling: structural reorganization governs the mechanical response of nanocellular polymers. *Polymers* **359**, 130302 (2026).

8. Gibson, L. J. & Ashby, M. F. The mechanics of three-dimensional cellular materials. *Proc. royal society London. A. Math. physical sciences* **382**, 43–59 (1982).

9. Aney, S., Pandit, P., Ratke, L., Milow, B. & Rege, A. On the origin of power-scaling exponents in silica aerogels. *J. Sol-Gel Sci. Technol.* **114**, 98–105 (2025).

10. Weigold, L. & Reichenauer, G. Correlation between mechanical stiffness and thermal transport along the solid framework of a uniaxially compressed polyurea aerogel. *J. non-crystalline solids* **406**, 73–78 (2014).

11. Aney, S. & Rege, A. Network decomposition model to describe the solid and gaseous thermal conductivity in open-porous (nano) materials. *Int. J. Heat Mass Transf.* **236**, 126316 (2025).

12. Gross, J. & Fricke, J. Ultrasonic velocity measurements in silica, carbon and organic aerogels. *J. Non-Crystalline Solids* **145**, 217–222 (1992).

13. Qin, Z., Jung, G. S., Kang, M. J. & Buehler, M. J. The mechanics and design of a lightweight three-dimensional graphene assembly. *Sci. advances* **3**, e1601536 (2017).

14. Zhao, S., Malfait, W. J., Guerrero-Alburquerque, N., Koebel, M. M. & Nyström, G. Biopolymer aerogels and foams: Chemistry, properties, and applications. *Angewandte Chemie Int. Ed.* **57**, 7580–7608 (2018).

15. Diascorn, N., Calas, S., Sallée, H., Achard, P. & Rigacci, A. Polyurethane aerogels synthesis for thermal insulation–textural, thermal and mechanical properties. *The J. Supercrit. Fluids* **106**, 76–84 (2015).

16. Lledó, J., Martín-de León, J., Álvarez-Arenas, T. G., Rodríguez-Pérez, M. & Merillas, B. Unraveling the structure-properties correlation in thermal insulating and mechanically stiff pla aerogels. *J. Mater. Res. Technol.* **36**, 641–652 (2025).

17. Filimonova, E. *et al.* Effect of polymer concentration and cross-linking density on the microstructure and properties of polyimide aerogels. *J. Sol-Gel Sci. Technol.* **110**, 747–759 (2024).

18. Meador, M. A. B. *et al.* Polyimide aerogels with amide cross-links: a low cost alternative for mechanically strong polymer aerogels. *ACS applied materials & interfaces* **7**, 1240–1249 (2015).

19. Steffens, K., Bialuschewski, D. & Milow, B. Tuning density and morphology of organic-inorganic hybrid-silica aerogels through precursor dilution for lightweight applications. *J. Sol-Gel Sci. Technol.* **112**, 768–775 (2024).

20. Groß, J. & Fricke, J. Scaling of elastic properties in highly porous nanostructured aerogels. *Nanostructured Mater.* **6**, 905–908 (1995).

21. Woignier, T., Phalippou, J. & Vacher, R. Parameters affecting elastic properties of silica aerogels. *J. Mater. Res.* **4**, 688–692 (1989).

22. Abdusalamov, R. *et al.* Modeling and simulation of the aggregation and the structural and mechanical properties of silica aerogels. *The J. Phys. Chem. B* **125**, 1944–1950 (2021).

23. Pekala, R., Alviso, C. & LeMay, J. Organic aerogels: microstructural dependence of mechanical properties in compression. *J. non-crystalline solids* **125**, 67–75 (1990).

24. Scherer, G. W., Smith, D. M., Qiu, X. & Anderson, J. M. Compression of aerogels. *J. Non-Crystalline Solids* **186**, 316–320 (1995).

25. Chandrasekaran, S. N., Näsholm, S. P. & Holm, S. Wave equations for porous media described by the biot model. *The J. Acoust. Soc. Am.* **151**, 2576–2586 (2022).

26. Prikazchikova, L., Rege, A. G., Kaplunov, J. & Prikazchikov, D. Low-frequency propagating and evanescent waves in strongly inhomogeneous sandwich plates. *Zeitschrift fur Angewandte Math. und Physik* **75**, 211 (2024).

27. Yadav, A. & Galich, P. I. Elastic wave propagation in isotropic magneto-active polymers. *Int. J. Mech. Sci.* 110730 (2025).

28. Luo, H., Malakooti, S., Churu, H. G., Leventis, N. & Lu, H. Mechanical characterization of aerogels. In *Springer handbook of aerogels*, 197–229 (Springer, 2022).

29. Merillas, B., Martín-de León, J., Villafañe, F. & Rodríguez-Pérez, M. Transparent polyisocyanurate-polyurethane-based aerogels: Key aspects on the synthesis and their porous structures. *ACS Appl. Polym. Mater.* **3**, 4607–4615 (2021).

30. Merillas, B., Villafañe, F. & Rodríguez-Pérez, M. Super-insulating transparent polyisocyanurate-polyurethane aerogels: Analysis of thermal conductivity and mechanical properties. *Nanomaterials* **12**, 2409 (2022).

31. Altarabeen, R. *et al.* Lignin polyurethane aerogels: Influence of solvent on textural properties. *Gels* **10**, 827 (2024).

32. Gay, S. *et al.* Pla scaffolds production from thermally induced phase separation: Effect of process parameters and development of an environmentally improved route assisted by supercritical carbon dioxide. *J. Supercrit. Fluids* **136**, 12–135 (2018).

33. Meador, M. A. B. *et al.* Mechanically strong, flexible polyimide aerogels cross-linked with aromatic triamine. *ACS applied materials & interfaces* **4**, 536–544 (2012).

34. Guo, H. *et al.* Poly (maleic anhydride) cross-linked polyimide aerogels: synthesis and properties. *RSC advances* **6**, 26055–26065 (2016).

35. Feng, J., Wang, X., Jiang, Y., Du, D. & Feng, J. Study on thermal conductivities of aromatic polyimide aerogels. *ACS Appl. Mater. & Interfaces* **8**, 12992–12996 (2016).

36. Fener, R. & Niemeyer, P. Flexible komposite auf basis von aerogelen. Tech. Rep. EP 3 042 884 B1, European Patent Office (2016).

37. Hayase, G., Kanamori, K., Kazuki, K. & Hanada, T. Synthesis of new flexible aerogels from mtms/dmdms via ambient pressure drying. *IOP Conf. Series: Mater. Sci. Eng.* **18** (2011).

38. Li, C. *et al.* Silica aerogels: from materials research to industrial applications. *Int. Mater. Rev.* **68**, 862–900 (2023).

39. Hua, D., Anderson, J., Di Gregorio, J., Smith, D. & Beaucage, G. Structural analysis of silica aerogels. *J. non-crystalline solids* **186**, 142–148 (1995).

40. Pollanen, J. *et al.* Globally anisotropic high porosity silica aerogels. *J. non-crystalline solids* **354**, 4668–4674 (2008).

41. Iswar, S. *et al.* Effect of aging on silica aerogel properties. *Microporous Mesoporous Mater.* **241**, 293–302 (2017).

42. Reichenauer, G. Structural characterization of aerogels. In *Springer Handbook of Aerogels*, 151–195 (Springer, 2023).

43. Pekala, R. Organic aerogels from the polycondensation of resorcinol with formaldehyde. *J. materials science* **24**, 3221–3227 (1989).

44. Schwan, M., Naikade, M., Raabe, D. & Ratke, L. From hard to rubber-like: mechanical properties of resorcinol–formaldehyde aerogels. *J. Mater. Sci.* **50**, 5482–5493 (2015).

45. Gross, J., Scherer, G. W., Alviso, C. T. & Pekala, R. W. Elastic properties of crosslinked resorcinol-formaldehyde gels and aerogels. *J. non-crystalline solids* **211**, 132–142 (1997).

46. Gross, J., Reichenauer, G. & Fricke, J. Mechanical properties of sio2 aerogels. *J. Phys. D: Appl. Phys.* **21**, 1447–1451 (1988).

47. Gómez Álvarez Arenas, T. Acoustic impedance matching of piezoelectric transducers to the air. ieee trans ultrason ferroelectr freq control. *IEEE Transactions on Ultrason. Ferroelectr. Freq. Control.* **51**, 624–633 (2004).

48. Kelly, S. P., Hayward, G. & Gómez Álvarez Arenas, T. Characterization and assessment of an integrated matching layer for air-coupled ultrasonic applications. *IEEE Transactions on Ultrason. Ferroelectr. Freq. Control.* **51**, 1314–1323 (2004).

Funding Declaration

No funding to report for this research.

Author contributions statement

A.R. and A.B. conceptualised the study, B.M., M.H-Z., P.H., M.S., and N.H.B. conducted the synthesis and density characterisation of the aerogels, A.R., B.M., and C.S. conducted sound velocity measurements, A.R. and A.B. conducted theoretical investigation, all authors contributed to analysing the results and writing and reviewing of the manuscript.